UDK 669.715:539.412
Original scientific article/Izvirni znanstveni članek

ISSN 1580-2949
Mater. Tehnol.

TENSILE DEFORMATION BEHAVIOR AND CONSTITUTIVE MODELING OF SOLID-SOLUTION-TREATED 6061 ALUMINUM ALLOY

OBNAŠANJE RAZTOPNO ŽARJENE ALUMINIJEVE ZLITINE TIPA 6061 POD NATEZNO OBREMENITVIJO IN POSTAVITEV KONSTITUTIVNEGA MODELA

Shanping Deng, Tao He*, Xiangyang Du, Jiayun Zhu

School of Mechanical and Automotive Engineering, Shanghai University of Engineering Science, Songjiang 201620, Shanghai, China

Prejem rokopisa – received: 2025-09-26; sprejem za objavo – accepted for publication: 2026-01-22

doi:10.17222/mit.2025.1572

To systematically investigate the tensile deformation behavior of solid-solution-treated 6061 aluminum alloy under varying temperatures and strain rates and to establish an applicable constitutive model, uniaxial tensile tests were conducted using a 68TM-50 universal tensile testing machine and a Gleeble-3800 thermomechanical simulator. The experiments covered a temperature range of 25–300 °C and strain rates of 0.001–0.1 s^{-1} to obtain true stress-strain data. The results indicate that, at a constant strain rate, the peak stress decreases significantly with increasing temperature, whereas at a constant temperature, the peak stress increases with the strain rate. Temperature exhibits a more pronounced influence on peak stress than strain rate. For room-temperature conditions (25 °C), the Swift model accurately predicts the deformation behavior, achieving an overall correlation coefficient (R) of 0.99846 and an average absolute relative error (AARE) of 1.41 %. For elevated temperatures (150 °C and 300 °C), a modified Johnson-Cook (J-C) model was developed by incorporating a quadratic polynomial strain-hardening term and a temperature-strain rate coupling factor, effectively integrating the effects of strain hardening, strain rate sensitivity, and thermal softening. The modified J-C model demonstrates robust predictive capability in the warm temperature regime, with an overall R of 0.99739 and an overall AARE of 5.29 %.

Keywords: 6061 aluminum alloy, temperature, strain rate, tensile deformation, constitutive model

Avtorji v članku opisujejo sistematično raziskavo obnašanja aluminijeve zlitine tipa 6061 pod vplivom natezne obremenitve. Na vzorcih preiskovane zlitine, ki je bila predhodno raztopno žarjena so izvajali enoosne natezne preskuse z uporabo univerzalnega nateznega preskusnega stroja 68TM-50 in termomehanskega simulatorja Gleeble-3800. Preizkuse so izvajali pri različnih temperaturah v območju med 25 °C in 300 °C ter hitrostih natezne deformacije med 0,001 in 0,1 s^{-1}, da bi dobili dejanske podatke o odvisnostih med napetostjo in deformacijo. Rezultati preizkusov so pokazali, da se pri konstantni hitrosti deformacije najvišja (vršna) napetost znatno zmanjša z naraščajočo temperaturo, medtem ko se pri konstantni temperaturi najvišja napetost povečuje s hitrostjo deformacije. Temperatura ima izrazitejši vpliv na najvišjo napetost kot pa na hitrost deformacije. Pri sobni temperaturi (25 °C) model Swift natančno napoveduje obnašanje deformacije, pri čemer se doseže skupni korelacijski koeficient (R) 0,99846 in povprečno absolutno relativno napako (AARE) 1,41 %. Za povišane temperature deformacije (150 °C in 300 °C) so avtorji razvili modificiran Johnson-Cookov (J-C) konstitutivni model z vključitvijo člena kvadratnega polinoma za deformacijsko utrjevanje in faktorja sklopitve *temperatura-deformacija*. S tem so avtorji učinkovio integrirali vpliv deformacijskega utrjevanja, občutljivost na hitrost deformacije in toplotno mehčanje. Modificiran J-C model kaže robustno napovedno sposobnost v režimu povišanih temperatur, s skupnim R 0,99739 in skupnim AARE 5,29 %.

Ključne besede: aluminijeva zlitina tipa 6061, temperatura, hitrost deformacije, natezna obremenitev in deformacija, konstitutivni model

1 INTRODUCTION

6061 aluminum alloy is one of the most extensively used aluminum alloys, valued for its high strength, good formability, and excellent corrosion resistance.[1–3] These properties make it indispensable in applications within the aerospace and automotive industries. Solid solution treatment, a process involving the dissolution of alloying elements into the aluminum matrix to form a uniform supersaturated solid solution, significantly enhances the material's plasticity and improves the stability and uniformity of its mechanical properties. It is a standard pre-treatment process employed to improve the formability of materials subjected to severe plastic deformation.[4–7] The solid-solution state is metastable and characterized by a supersaturated microstructure. During deformation, simultaneous microstructural evolution processes – such as dislocation slip, dynamic recovery, and dynamic precipitation – occur, leading to flow stress behaviors distinct from those of stable states. These concurrent processes lead to flow stress behaviors that differ significantly from those of stable states.[8,9] Specifically, unlike stable states, the solid-solution matrix is unstable at elevated temperatures, where precipitates form and grow during deformation. This makes the flow stress highly sensitive to temperature and strain rate, limiting

*Corresponding author's e-mail:
hetao@sues.edu.cn (Tao HE)

the applicability of standard constitutive models. Consequently, directly applying constitutive models developed for stable-state materials can result in considerable deviations. Therefore, the development of a constitutive model capable of accurately predicting the mechanical response of solid-solution-treated 6061 aluminum alloy is crucial, particularly given its excellent plastic forming capabilities.

Various constitutive models have been extensively studied. Among them, the Swift model is notable for its simplicity and the clear physical meaning of its parameters, enabling an accurate description of the stress-strain relationship during plastic deformation, particularly at room temperature.[10–12] Gao et al. successfully fitted the room-temperature stress-strain curve of 6063 aluminum alloy using the Swift model and validated its predictive accuracy through finite element simulation.[13] Zhang et al. demonstrated that a modified Swift model for 304L stainless steel exhibited high agreement with experimental data at low temperatures.[14] Zhu et al. found that the Swift model effectively captures the isotropic strain hardening behavior of 6061 aluminum alloy prior to necking at room temperature.[15] Collectively, these studies indicate that the Swift model generally provides high precision in predicting material deformation behavior at room temperature.

However, the Swift model has limitations in characterizing the effects of temperature and strain rate, which are critical under warm forming conditions. In contrast, the Johnson-Cook (J-C) model incorporates separate terms for temperature and strain rate sensitivity, enabling a more comprehensive description of the quantitative relationships among flow stress, plastic strain, temperature, and strain rate, thereby making it more suitable for modeling under complex thermo-mechanical conditions.[16–19] For example, Ni et al. developed a modified J-C model for 6061-T6 aluminum alloy that more accurately describes its stress-strain response within the temperature range of 200–300 °C across various strain rates.[20] Similarly, Shen et al. successfully captured the tensile deformation behavior of 6061 aluminum alloy sheets under warm conditions using a modified J-C approach.[21] Fan et al. experimentally determined the key parameters of the J-C model for warm conditions,

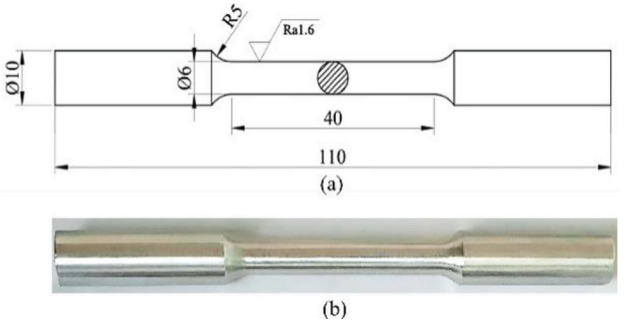

Figure 1: Tensile specimen: a) dimensions of the specimen; b) prepared tensile specimen

achieving accurate predictions of the mechanical response of 6061 aluminum alloy.[22] These studies collectively demonstrate the efficacy of the J-C model for predicting deformation behavior under warm conditions.

A key limitation of the standard J-C model lies in its assumption that strain hardening, strain rate sensitivity, and thermal softening act independently. This assumption is often invalid for materials like solid-solution-treated 6061 aluminum alloy under warm conditions. Due to its metastable nature, this alloy exhibits highly nonlinear flow stress behavior, accompanied by dynamic recovery and even dynamic precipitation during deformation.[23–25] Consequently, its mechanical response significantly differs from that of stable states (e.g., aged or annealed) and demonstrates a stronger, more complex dependence on both temperature and strain rate. Therefore, a constitutive model that effectively couples these three interdependent influences is essential for accurately predicting its mechanical response.

Building upon this background, the present study aims to develop constitutive models for solid-solution-treated 6061 aluminum alloy to characterize its tensile deformation behavior under a range of temperatures (25, 150, and 300) °C and strain rates (0.001, 0.01, and 0.1) s^{-1}. The influence of these parameters on the mechanical properties is quantitatively investigated through uniaxial tensile tests. A segmented modeling strategy is adopted. For room-temperature deformation, the Swift model is employed for its demonstrated accuracy in predicting uniform plastic deformation under these conditions. For elevated temperatures (150–300 °C), a modified Johnson-Cook model is developed to more reliably capture the coupled effects of strain hardening, strain rate sensitivity, and thermal softening. This approach provides targeted theoretical support for the process design and performance prediction of this alloy across its relevant processing temperature ranges.

2 MATERIALS AND METHODS

The material studied was a 6061 aluminum alloy that underwent solid-solution treatment at 540 °C for 1 h, followed by water quenching. The tensile deformation behavior of the treated alloy was investigated across a range of temperatures and strain rates. Uniaxial tensile tests were performed at room temperature (25 °C) and at elevated temperatures of 150 °C and 300 °C. For each temperature, strain rates of (0.001, 0.01, and 0.1) s^{-1} were applied, resulting in a total of nine experimental conditions, as summarized in **Table 1**. The geometry and dimensions of the tensile specimen are illustrated in **Figure 1a**, with a gauge length of 40 mm; a representative fabricated specimen is shown in **Figure 1b**.

All room-temperature tests were conducted on a 68TM-50 universal tensile testing machine. Elevated-temperature tests were performed on a Gleeble-3800 thermomechanical simulator. For the high-temperature

Table 1: 6061 aluminum alloy tensile test parameters

Temperature (°C)	25			150			300		
Strain rate (s^{-1})	0.001	0.01	0.1	0.001	0.01	0.1	0.001	0.01	0.1

tests, specimens were resistance-heated to the target temperature at a rate of 5 °C/s and held for 180 s to ensure a uniform thermal distribution prior to tensile loading until fracture. Following fracture, all specimens tested at elevated temperatures were air-cooled to room temperature.

3 RESULTS AND DISCUSSION

3.1 Room temperature deformation behavior and constitutive modeling

3.1.1 Analysis of room temperature deformation behavior

The true stress-true strain curves obtained from room-temperature tensile tests are presented in **Figure 2a**. These curves indicate that the flow stress level generally increases with the strain rate over the tested range of 0.001–0.1 s^{-1}. Specifically, at a constant true strain, the true stress is higher for a higher strain rate. This positive strain rate sensitivity is further quantified by the peak stress data plotted in **Figure 2b**. The peak stress of the solid-solution-treated 6061 aluminum alloy exhibits a clear positive correlation with the strain rate. For instance, an increase in the strain rate from 0.001 s^{-1} to 0.01 s^{-1} resulted in a rise in the peak stress from 223.26 MPa to 226.83 MPa, corresponding to an increase of 1.60 %. A further increase in the strain rate from 0.01 s^{-1} to 0.1 s^{-1} caused the peak stress to rise to 231.64 MPa, representing a larger incremental change of 3.75 %. This observed mechanical response can be attributed to the influence of strain rate on dislocation dynamics. A higher strain rate entails a larger plastic strain increment per unit time, which activates a greater number of dislocations and promotes their slip. Consequently, the dislocation density increases at higher strain rates, leading to more intense interactions between dislocations. These interactions, such as entanglement and formation of junctions, increase the resistance to dislocation motion, thereby enhancing the material's flow stress and its overall resistance to plastic deformation.[26,27]

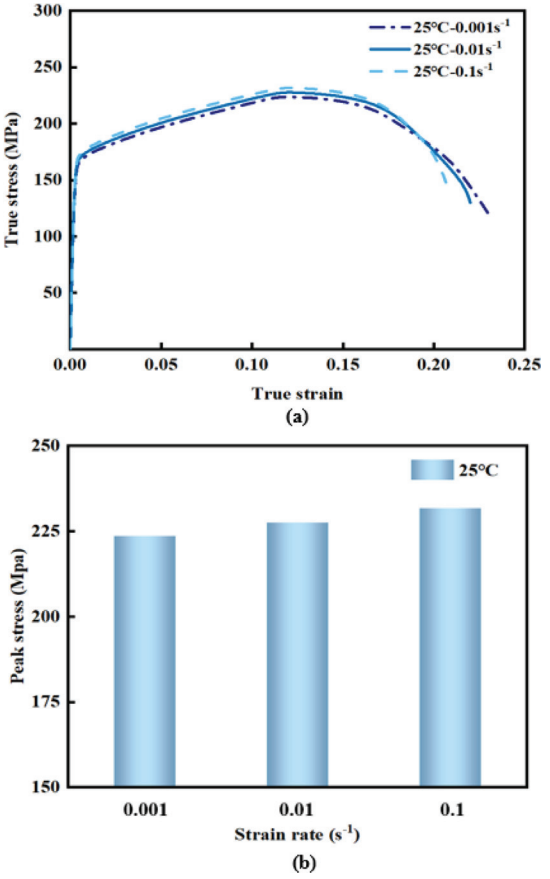

Figure 2: Room temperature tensile test results: a) true stress-true strain curves under different strain rates; b) peak stress values under different strain rates

3.1.2 Establishment and validation of room temperature constitutive model

Based on the tensile performance test results in **Figure 2**, the true stress-true strain curves of the solid-solution-treated 6061 aluminum alloy at 25 °C exhibit stable work-hardening characteristics. The metastable nature of the material is not significantly activated, and the increase in the peak stress with the strain rate is relatively small. Thus, its plastic deformation behavior can be accurately described without introducing complex strain rate correction terms. Accordingly, this study selected the Swift model for constitutive modeling under room temperature conditions. Its expression is shown in Equation (1):[10]

$$\sigma = K(\varepsilon_0 + \varepsilon_p)^n \quad (1)$$

Here, K is the strength coefficient, ε_0 is the initial yield offset strain, ε_p is the plastic strain, and n is the strain hardening exponent.

The fitting process used uniaxial tensile test data at 25 °C and a strain rate of 0.01 s^{-1}. The elastic stage and the necking unloading stage were removed from the data to obtain the true stress-true strain curve representing the tensile plastic deformation stage. Nonlinear parameter fitting for the Swift model was performed using the least squares method. The fitting result is shown in **Figure 3**, and the resulting Swift model formula is given by Equation (2):

$$\sigma = 323.261(0.022 + \varepsilon_p)^{0.78} \quad (2)$$

The predictive accuracy of the developed constitutive model was evaluated by comparing model predictions with experimental data. Two statistical metrics were em-

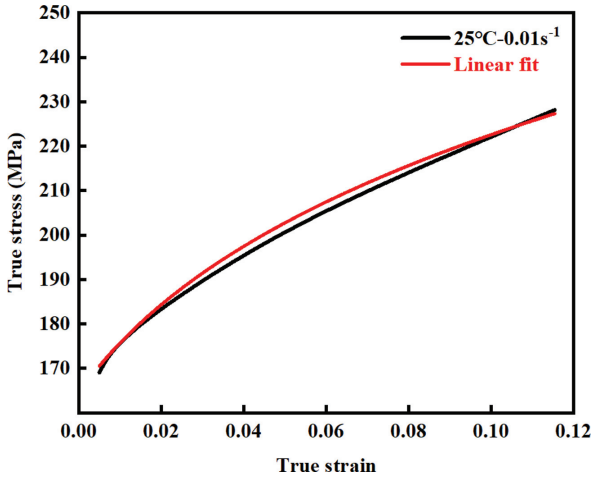

Figure 3: Fitting curve of the Swift model

ployed to quantify the prediction accuracy: the correlation coefficient (R) and the average absolute relative error (AARE). The formulations for these metrics are provided in Equations (3) and (4), respectively.

$$R = \frac{\sum_{i=1}^{N}(E_i - \overline{E})(P_i - \overline{P})}{\sqrt{\sum_{i=1}^{N}(E_i - \overline{E})^2 \sum_{i=1}^{N}(P_i - \overline{P})^2}} \quad (3)$$

$$AARE = \frac{1}{N}\sum_{i=1}^{N}\left|\frac{E_i - P_i}{E_i}\right| \times 100\% \quad (4)$$

Here, E_i is the value of the experimental data point, P_i is the corresponding model predicted value, $\overline{E}$ is the average value of all experimental data, $\overline{P}$ is the average value of all predicted data, and N is the total number of data points. The correlation coefficient R measures the strength of the linear correlation between predicted and experimental values; the closer its value is to 1, the stronger the correlation. The AARE quantifies the relative magnitude of the prediction error. The smaller its value, the higher the prediction accuracy of the model.

A comparison between the experimental data and model predictions is presented in **Figure 4a**, which shows minor deviations, indicating that the Swift model accurately predicts the tensile deformation behavior of the solid-solution-treated 6061 aluminum alloy at room temperature. This conclusion is further supported by the linear correlation plot in **Figure 4b**, where the data points from all strain rates cluster closely around the ideal fit line ($y = x$), demonstrating a strong linear correlation between the predicted and experimental values. The quantitative prediction accuracy of the model is summarized in **Table 2**. The model achieves an overall correlation coefficient (R) of 0.99846 and an average absolute relative error ($AARE$) of only 1.41 % across all tested strain rates, indicating excellent global accuracy. Analysis of the error variation with strain rate reveals that the prediction accuracy is highest at a strain rate of 0.01 s^{-1}, with an R value of 0.99788 and an $AARE$ of 0.557 %, representing the smallest error among all test conditions. This suggests that the model most accurately captures the strain hardening characteristics of the material during uniform plastic deformation at this specific strain rate. At the lower strain rate of 0.001 s^{-1}, the R value remains high at 0.99820, while the $AARE$ increases slightly, to 1.994 %. At the higher strain rate of 0.1 s^{-1}, the values (R = 0.99726, $AARE$ = 1.529 %) fall between those observed at the other two strain rates. Despite these minor variations, the prediction accuracy remains high across the entire range of strain rates investigated.

These results demonstrate that the Swift model provides highly accurate predictions for the room-temperature deformation behavior of solid-solution-treated 6061 aluminum alloy. Although the prediction accuracy exhibits a slight dependence on strain rate, it consistently remains within a range that is acceptable for engineering applications, thereby verifying the reliability of the model.

Table 2: Prediction accuracy of the Swift model

Model	Temperature (°C)	Strain rate (s^{-1})	R	$AARE$ (%)
Swift	25	0.001	0.99820	1.994
	25	0.01	0.99788	0.557
	25	0.1	0.99726	1.529
	25	Overall	0.99846	1.410

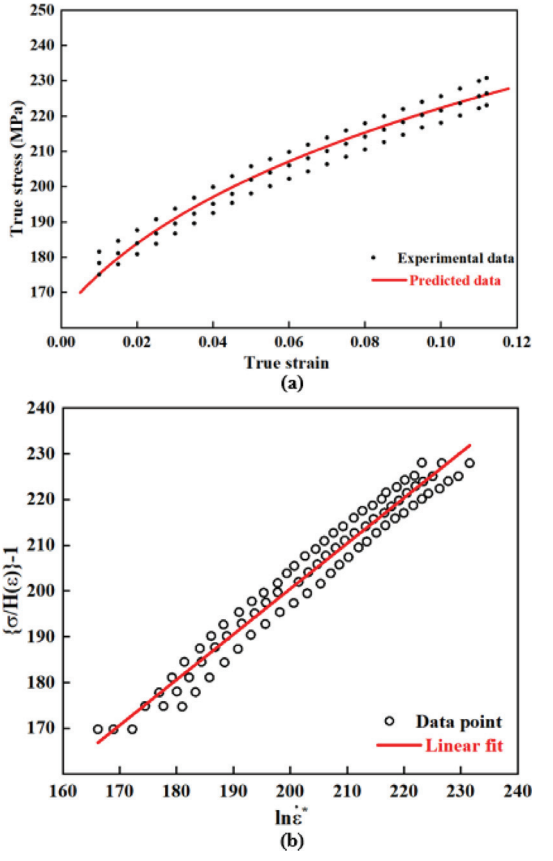

Figure 4: Prediction results and accuracy evaluation of the Swift model: a) comparison between experimental data and model predicted data; b) linear fit and accuracy evaluation

3.2 Warm temperature deformation behavior and constitutive modeling

3.2.1 Analysis of warm temperature deformation behavior

The true stress–true strain curves obtained under warm conditions are presented in **Figure 5a**, illustrating the flow stress behavior of the solid-solution-treated 6061 aluminum alloy. A clear influence of temperature is evident, as the flow stress levels at 300 °C are significantly lower than those at 150 °C. This trend is further quantified by the peak stress data summarized in **Figure 5b**, which demonstrates that the peak stress increases with increasing strain rate at a constant temperature. Specifically, at 150 °C, the peak stress increased continuously from 172.37 MPa to 185.35 MPa as the strain rate was raised from 0.001 s^{-1} to 0.1 s^{-1}, representing a total increase of approximately 7.53 %. A more pronounced strain rate sensitivity was observed at 300 °C, where the peak stress increased from 99.48 MPa to 115.79 MPa over the same strain rate range, corresponding to a larger total increase of 16.39 %. This mechanical response can be attributed to the competing effects of strain hardening and thermal activation. An increase in the strain rate raises the frequency and density of dislocation motion, thereby accelerating the work hardening rate and leading to higher flow stresses. Conversely, thermally-activated softening mechanisms – such as dislocation climb and cross-slip – require time to operate. At higher strain rates, the available time for these recovery processes is reduced, causing them to lag behind the deformation process. This relative suppression of thermal softening results in the observed increase in peak stress with strain rate.[28]

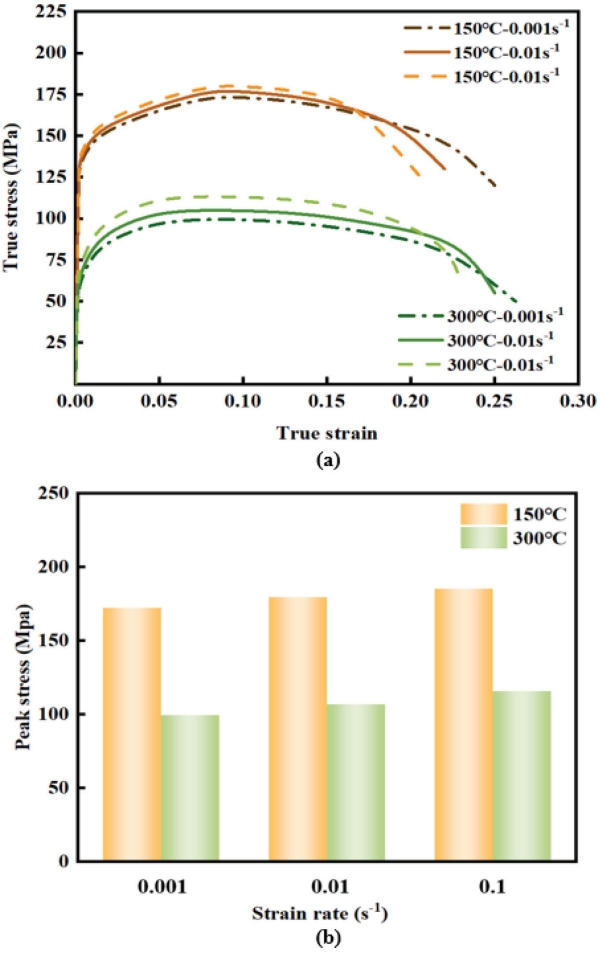

Figure 5: Warm temperature tensile test results: a) true stress-true strain curves at different temperatures and strain rates; b) peak stress values at different temperatures and strain rates

Conversely, at a fixed strain rate, the peak stress exhibits a strong negative dependence on temperature. This thermal softening effect is clearly demonstrated by the data in **Figure 5b**. For instance, at a constant strain rate of 0.001 s^{-1}, increasing the temperature from 150 °C to 300 °C resulted in a sharp decline in the peak stress from 172.37 MPa to 99.48 MPa, corresponding to a substantial reduction of 42.29 %. This trend is consistent across all tested strain rates: at 0.01 s^{-1}, the peak stress decreased from 179.51 MPa to 106.94 MPa (a 40.43 % reduction), and at 0.1 s^{-1}, it decreased from 185.35 MPa to 115.79 MPa (a 37.53 % reduction). This pronounced thermal softening behavior is fundamentally governed by thermally activated processes. An increase in temperature reduces the activation energy required for atomic diffusion and dislocation motion. This enhancement of atomic mobility significantly accelerates key softening mechanisms, most notably dynamic recovery and dynamic recrystallization. These thermally activated processes operate more efficiently at elevated temperatures, thereby more effectively counteracting the competing work hardening.[29,31] Consequently, the flow stress required to sustain plastic deformation is markedly reduced, leading to the observed sharp decrease in peak stress with increasing temperature.

3.2.2 Establishment and validation of warm temperature constitutive model

To describe the deformation behavior of the solid-solution-treated 6061 aluminum alloy under warm conditions, a modified Johnson-Cook (J-C) constitutive model was developed. Unlike the standard J-C model, the present modification incorporates a quadratic polynomial function to represent the strain hardening response. Furthermore, it introduces coupling factors within the strain rate and temperature softening terms to account for the synergistic interactions among strain hardening, strain rate sensitivity, and thermal softening.[32] The expression for the modified constitutive model is given by Equation (5):

$$\sigma = (A_2\varepsilon^2 + A_1\varepsilon + A_0)(1 + B_1 \ln\dot{\varepsilon}^*)e^{\left[(C_1 + C_0 \ln\dot{\varepsilon}^*)(T - T_0)\right]} \quad (5)$$

Here, A_2, A_1, A_0, B_1, C_1 and C_0 are material constants to be determined, σ is the flow stress, ε is the equivalent plastic strain, T is the current temperature, T_0 is the reference temperature, and $\dot{\varepsilon}^* = \dot{\varepsilon}/\dot{\varepsilon}_0$ is the dimensionless

strain rate, where $\dot{\varepsilon}$ is the current strain rate and $\dot{\varepsilon}_0$ is the reference strain rate. Physically, this coupling term indicates that thermal softening takes time. Microstructural changes like dynamic precipitation and recovery are not instantaneous. At high strain rates, deformation happens too quickly for these processes to fully occur, effectively suppressing the softening effect. This term captures the rate-dependent behavior.

Prior to fitting, the reference strain rate $\dot{\varepsilon}_0$ and reference temperature T_0 needed to be set. Based on the coverage of the test conditions and the data points, the reference strain rate $\dot{\varepsilon}_0$ was selected as 0.001 s^{-1}, thus $\dot{\varepsilon}^* = 1$, 10, 100. The reference temperature T_0 was selected as 150 °C, making $T - T_0$ equal to 0 at this temperature. To determine the strain hardening parameters A_0, A_1 and A_2 data from the uniform plastic deformation stage were used, where the material undergoes homogeneous deformation prior to necking. In this stage, the material has not yet undergone significant necking or inhomogeneous deformation, better reflecting the material's inherent hardening characteristics. The hardening term is expressed by Equation (6):

$$H(\varepsilon) = (A_2\varepsilon^2 + A_1\varepsilon + A_0) \quad (6)$$

Under this reference condition, the true stress-true strain experimental data were fitted using Equation (6). The fitting result is shown in **Figure 6**. It can be observed that the overall fitting error is small. The obtained values are A_2 = –5242.832 MPa, A_1 = 899.115 MPa, and A_0 = 138.670 MPa.

Following the determination of the strain hardening parameters A_0, A_1 and A_2 the subsequent step involved calibrating the parameters for the strain rate sensitivity term and the thermal softening term. This calibration was performed using the tensile test data obtained at the reference temperature across three strain rates (0.001, 0.01, and 0.1) s^{-1}. With the reference temperature fixed at 150 °C, the strain hardening term H(e) in the strain rate sensitivity model was thus determined by fitting the model in the form of Equation (7):

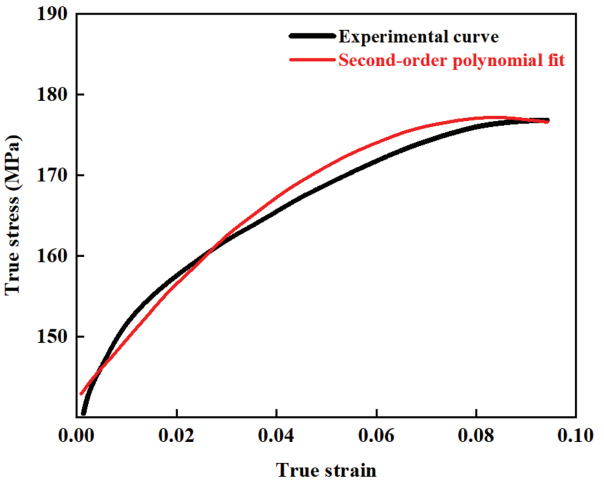

Figure 6: Fitting curve of the strain hardening term $H(\varepsilon)$

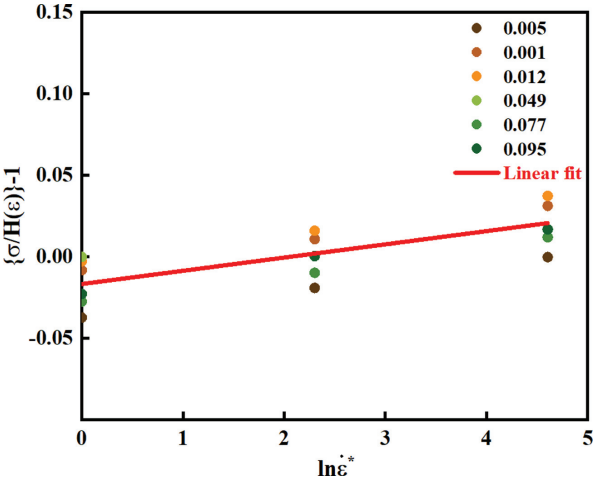

Figure 7: Linear fitting for parameter B_1

$$\sigma = H(\varepsilon)(1 + B_1 \ln\dot{\varepsilon}^*) \quad (7)$$

To determine the strain rate parameter, Equation (7) was linearized to obtain Equation (8):

$$\sigma / H(\varepsilon) - 1 = B_1 \ln\dot{\varepsilon}^* \quad (8)$$

By plotting the scatter diagram of $\sigma / H(\varepsilon) - 1$ versus $\ln\dot{\varepsilon}^*$ and performing linear regression fitting, the slope obtained is the value of B_1. The fitting result is shown in **Figure 7**. The value of the strain rate parameter B_1 was found to be 0.00872. Therefore, the strain rate modification can be expressed as Equation (9):

$$S(\dot{\varepsilon}^*) = 1 + B_1 \ln\dot{\varepsilon}^* = 1 + 0.00872 \ln\dot{\varepsilon}^* \quad (9)$$

After determining the parameters for the strain rate modification term and the strain hardening term, the model formula (5) can be further rearranged into Equation (10):

$$\sigma / H(\varepsilon) S(\dot{\varepsilon}^*) = e^{\left[(C_0 + C_1 \ln\dot{\varepsilon}^*)(T - T_0)\right]} \quad (10)$$

Taking the natural logarithm of both sides of the equation yields Equation (11):

$$\ln\left\{\sigma / H(\varepsilon) S(\dot{\varepsilon}^*)\right\} = (C_1 + C_0 \ln\dot{\varepsilon}^*)(T - T_0) \quad (11)$$

Letting $C^* = C_1 + C_0 \ln\dot{\varepsilon}^*$, it can be seen that $\ln\left\{\sigma / H(\varepsilon) S(\dot{\varepsilon}^*)\right\}$ exhibits a linear relationship with $T - T_0$, and its slope depends on the strain rate $\dot{\varepsilon}^*$. Using the tensile test data at different temperatures, the corresponding values of $\ln\left\{\sigma / H(\varepsilon) S(\dot{\varepsilon}^*)\right\}$ were calculated. As shown in **Figure 8**, to determine the coupling parameters under warm conditions, scatter plots of $\ln\left\{\sigma / H(\varepsilon) S(\dot{\varepsilon}^*)\right\}$ versus $T - T_0$ were plotted for each strain rate $\dot{\varepsilon}^*$, and linear fitting was performed. The slope of the fitted line is the value of °C at that strain rate. When the value of $\dot{\varepsilon}^*$ is 1, C^* = –0.0050, and the fitting result is shown in **Figure 8a**. When $\dot{\varepsilon}^*$ is 10, C^* = –0.00313, and the fitting result is shown in **Figure 8b**. When $\dot{\varepsilon}^*$ is 100, C^* = –0.00294, and the fitting result is shown in **Figure 8c**. The obtained three ($\ln\dot{\varepsilon}^*$, C^*) data points were subjected to linear fitting. The fitted linear

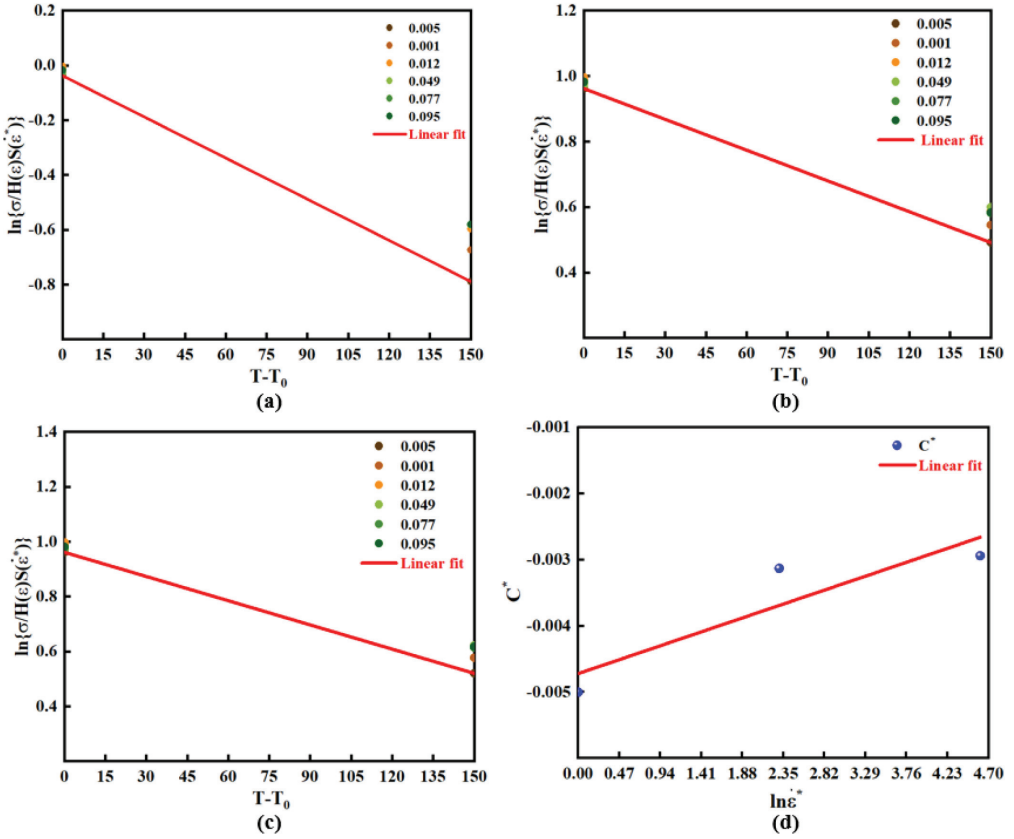

Figure 8: Determination of coupling term parameters: a) $\dot{\varepsilon}^* = 1$; b) $\dot{\varepsilon}^* = 10$; c) $\dot{\varepsilon}^* = 100$; d) linear fitting of c versus $\ln \dot{\varepsilon}^*$

equation is $C^* = C_1 + C_0 \ln \dot{\varepsilon}^*$. By solving this linear regression equation, the values of the coupling coefficients C_0 and C_1 could be obtained. The fitting result is shown in **Figure 8d**. The values were determined as C_1 = –0.00472 and C_0 = 0.00044732. The final constitutive equation applicable to the warm tensile deformation of solid-solution-treated 6061 aluminum alloy is shown in Equation (12):

$$\sigma = (-5242.832 \cdot \varepsilon^2 + 899.115 \cdot \varepsilon + 138.670) \cdot (1 + 0.00872 \ln \dot{\varepsilon}^*) \cdot e^{\left[(-0.00472 + 0.00044732 \ln \dot{\varepsilon}^*)(T-150)\right]} \quad (12)$$

The predictive capability of the modified Johnson-Cook model is demonstrated in **Figures 9a–c**, which compare the predicted and experimental true stress-true strain curves at 150 and 300 °C across various strain rates. A high degree of visual agreement is observed between the model predictions and the experimental data. Notably, the model accurately captures the material's response during the uniform plastic deformation stage, with minimal deviation from the experimental values. This close agreement confirms the model's effectiveness in representing the coupled effects of strain hardening, strain rate sensitivity, and thermal softening within this temperature regime. This quantitative agreement is further substantiated by the correlation plot in **Figure 9d**, where the data points are closely distributed along the ideal prediction line ($y = x$), indicating a strong linear correlation between the predicted and experimental values. The overall prediction accuracy, quantified by the statistical metrics from **Table 3**, is excellent, with an overall correlation coefficient (R) of 0.99739 and an average absolute relative error (AARE) of 5.29 %.

A detailed analysis of the prediction accuracy reveals consistent performance across different test conditions. At 150 °C, all R values exceed 0.989, and the AARE remains within a narrow range of 1.853–2.340 %. The highest accuracy at this temperature was achieved at 0.1 s^{-1}, with an R value of 0.99748 and an AARE of 1.963 %. At 300 °C, the model maintains good predictive capability. The accuracy is highest at the lowest strain rate (0.001 s^{-1}), with an R of 0.97652 and an exceptionally low AARE of 1.702 %. At higher strain rates of 0.01 s^{-1} and 0.1 s^{-1}, the R values are 0.95225 and 0.96239, with AARE values of 3.014 % and 3.402 %, respectively. It is noted that the prediction error increases slightly at 300 °C. This occurs because significant thermal softening interferes with the strain hardening process at higher temperatures. This complex interplay makes the stress-strain curve shape harder to characterize mathematically. Despite this, the model maintains good overall reliability.

In summary, the modified Johnson-Cook model – through its incorporation of a quadratic strain-hardening function and coupled temperature-strain rate terms – demonstrates robust and stable predictive performance

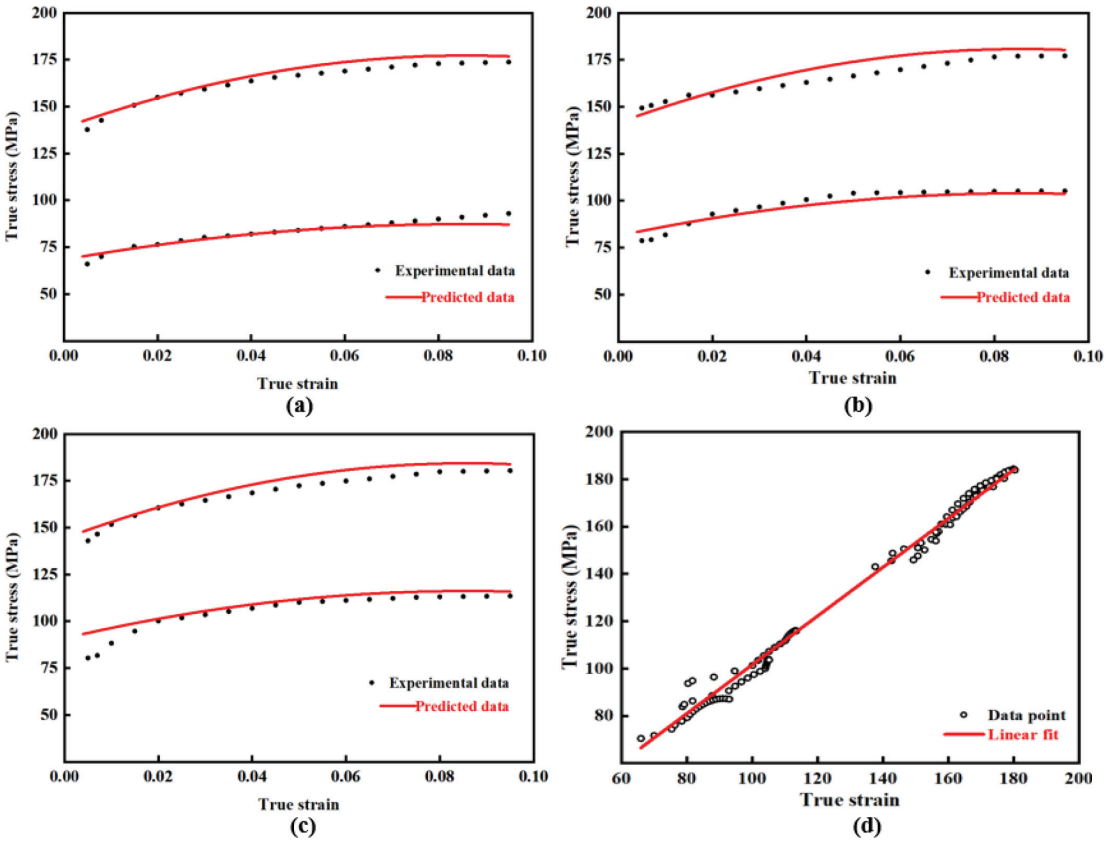

Figure 9: Prediction results and accuracy evaluation of modified J-C model: a) strain rate of 0.001 s^{-1}; b) strain rate of 0.01 s^{-1}; c) strain rate of 0.1 s^{-1}; (d) linear fit and accuracy evaluation

across the warm forming temperature range of 150–300 °C. The model provides reliable theoretical support for the design and optimization of warm forming processes for solid-solution-treated 6061 aluminum alloy.

Table 3: Prediction accuracy of modified J-C model

Model	Temperature (°C)	Strain rate (s^{-1})	R	AARE (%)
Modified J-C	150	0.001	0.99110	1.853
	150	0.01	0.98953	2.340
	150	0.1	0.99748	1.963
	300	0.001	0.97652	1.702
	300	0.01	0.95225	3.014
	300	0.1	0.96239	3.402
	Overall	Overall	0.99739	5.290

4 CONCLUSIONS

(1) The tensile deformation behavior of solid-solution-treated 6061 aluminum alloy exhibits significant dependence on both temperature and strain rate. A strong thermal softening effect is observed, where the peak stress decreases markedly with increasing temperature at constant strain rate. Conversely, the material demonstrates positive strain rate sensitivity, with peak stress increasing with strain rate at constant temperature. Comparative analysis reveals that temperature exerts a more pronounced influence on peak stress than strain rate.

(2) For room-temperature (25 °C) deformation, the Swift model provides accurate predictions of the tensile deformation behavior. The model achieves an excellent overall correlation coefficient (R) of 0.99846 and a low average absolute relative error (AARE) of 1.41 %, demonstrating its high predictive accuracy for uniform plastic deformation under these conditions.

(3) For elevated temperature conditions (150–300 °C), a modified Johnson-Cook constitutive model was developed. This enhanced formulation incorporates a quadratic polynomial strain-hardening term and introduces coupling factors to account for the synergistic interactions between temperature and strain rate effects. The model effectively integrates the coupled effects of strain hardening, strain rate sensitivity, and thermal softening, exhibiting robust predictive capability across the warm forming temperature range. This is evidenced by its high overall correlation coefficient (R = 0.99739) and acceptable predictive error (AARE = 5.29 %).

Acknowledgements

This work was supported by the National Natural Science Foundation of China (Grant No.52275350) and International cooperative scientific research platform of SUES (Grant No.0301006).

Contributions

Shanping DENG (ORCID: 0009-0004-2603-7888): Data curation, Methodology, Investigation, Writing-original draft. Tao HE: Funding acquisition, Supervision, Project administration, Writing-review & editing. Xiangyang DU: Writing-review & editing. Jiayun ZHU: Writing-review & editing.

Competing interests

All contributing authors hereby affirm that they have no conflicts of interest pertaining to this study. We reiterate our unequivocal declaration that there are no conflicts of interest associated with the submitted work, including any commercial or ancillary interests.

5 REFERENCES

[1] N. K. Chandla, S. Kant, M. M. Goud, Mechanical, tribological and microstructural characterization of stir cast Al-6061 metal/matrix composites—a comprehensive review, Sādhanā, 46 (**2021**) 1, 47, doi:10.1007/s12046-021-01567-7

[2] H. Demir, S. Gündüz, The effects of aging on machinability of 6061 aluminium alloy, Materials & Design, 30 (**2009**) 5, 1480–1483, doi:10.1016/j.matdes.2008.08.007

[3] D. Maisonnette, M. Suery, D. Nelias, P. Chaudet, T. Epicier, Effects of heat treatments on the microstructure and mechanical properties of a 6061 aluminium alloy, Materials Science and Engineering: A, 528 (**2011**) 6, 2718–2724, doi:10.1016/j.msea.2010.12.011

[4] J. Li, T. He, X. Du, A. Vereschaka, J. Zhang, Regulating hardness homogeneity and corrosion resistance of Al-Zn-Mg-Cu alloy via ECAP combined with inter-pass aging, Materials Characterization, 218 (**2024**), 114489, doi:10.1016/j.matchar.2024.114489

[5] S. Yao, Q. Tang, J. Yang, C. Wang, H. Sun, R. Rong, H. Sun, G. Chu, Microstructural characterization and mechanical properties of 6061 aluminum alloy processed with short-time solid solution and aging treatment, Journal of Alloys and Compounds, 960 (**2023**), 170704, doi:10.1016/j.jallcom.2023.170704

[6] J. Li, T. He, X. Du, A. Vereschaka, Enhancing the corrosion resistance of high-strength Al-Zn-Mg-Cu alloys after equal channel angular pressing by developing retrogression and re-aging strategies, Corrosion Science, 246 (**2025**), 112736, doi:10.1016/j.corsci.2025.112736

[7] J. Zhang, T. He, X. Du, A. Vereschaka, M. Song, X. Chen, J. Li, Effect of pre-heat treatment and subsequent ECAP-CU on microstructure and corrosion behavior of 7075 Al alloy fasteners, Journal of Central South University, 32 (**2025**) 7, 2383–2403, doi:10.1007s11771-025-5987-2

[8] P. Nageswara, R. Jayaganthan, Effects of warm rolling and ageing after cryogenic rolling on mechanical properties and microstructure of Al 6061 alloy, Materials & Design, 39 (**2012**), 226–233. doi:10.1016/j.matdes.2012.02.010

[9] D. Jia, T. He, M. Song, Y. Huo, H. Hu, Effects of equal channel angular pressing and further cold upsetting process to the kinetics of precipitation during aging of 7050 aluminum alloy, Journal of Materials Research and Technology, 26 (**2023**), 5126–5140. doi:10.1016/j.jmrt.2023.08.258

[10] H. W. Swift, Plastic instability under plane stress, Journal of the Mechanics and Physics of Solids, 1 (**1952**) 1, 1–18, doi:10.1016/0022-5096(52)90002-1

[11] J. Zhu, T. He, X. Chen, X. Du, A. Vereschaka, J. Li, S. Deng, Optimization and influence of process parameters on ECAD section shrinkage of 7075 Al alloy, Materials and Technology, 59 (**2025**) 3, 403–413, doi:10.17222/mit.2024.1342

[12] N. Balaramakrishna, R. K. Kumar, A study on the estimation of SWIFT model parameters by finite element analysis, Proceedings of the Institution of Mechanical Engineers, Part D: Journal of Automobile Engineering, 223 (**2009**) 10, 1283–1300, doi:10.1243/09544070JAUTO1024

[13] J. Gao, T. He, Y. Huo, M. Song, T. Yao, W. Yang, Study on plastic damage of ECAP based on Bai-Wierzbicki criterion, Journal of Plasticity Engineering, 28 (**2021**) 2, 52–62, doi:10.3969/j.issn.1007-2012.2021.02.008

[14] J. Zhang, G. Cao, Z. Gu, Z. Wang, Y. Jin, J. Liu, The modified Swift constitutive model of 304L stainless steel at the cryogenic temperature based on the Olson–Cohen model, Engineering Fracture Mechanics, 307 (**2024**), 110336, doi:10.1016/j. engfracmech.2024.110336

[15] P. Zhu, Q. Zhang, H. Xu, Y. Ouyang, Experimental and numerical investigation on plasticity and fracture behaviors of aluminum alloy 6061-T6 extrusions, Archives of Civil and Mechanical Engineering, 21 (**2021**) 3, 88, doi:10.1007/s43452-021-00225-3

[16] G. R. Johnson, W. H. Cook, Fracture characteristics of three metals subjected to various strains, strain rates, temperatures and pressures, Engineering Fracture Mechanics, 21 (**1985**) 1, 31–48, doi:10.1016/0013-7944(85)90052-9

[17] W. K. Rule, S. E. Jones, A revised form for the Johnson–Cook strength model, International Journal of Impact Engineering, 21 (**1998**) 8, 609–624, doi:10.1016/j.msea.2010.07.061

[18] D. Zhang, Q. Shangguan, C. Xie, F. Liu, A modified Johnson-Cook model of dynamic tensile behaviors for 7075-T6 aluminum alloy, Journal of Alloys and Compounds, 619 (**2015**), 186–194, doi:10.1016/j.jallcom.2014.09.002

[19] D. Umbrello, R. M'saoubi, J. C. Outeiro, The influence of Johnson–Cook material constants on finite element simulation of machining of AISI 316L steel, International Journal of Machine Tools and Manufacture, 47 (**2007**) 3–4, 462–470, doi:10.1016/j.ijmachtools.2006.06.006

[20] S. Ni, Y. Wang, Q. Huang, Y. Cai, Y. Xie, Optimization of Process Parameters for Hot Forming of 6061 Aluminum Alloy Thin-walled Part Based on Improved J-C Constitutive Model, Aeronautical Manufacturing Technology, 68 (**2025**) 6, 78–85, doi:10.16080/j.issn1671-833x.2025.06.078

[21] W. Shen, F. Xue, C. Li, Y. Liu, X. Mo, Q. Gao, Study on constitutive relationship of 6061 aluminum alloy based on Johnson-Cook model, Materials Today Communications, 37 (**2023**), 106982, doi:10.1016/j.mtcomm.2023.106982

[22] X. Fan, T. Suo, Q. Sun, T. Wang, Dynamic mechanical behavior of 6061 Al alloy at elevated temperatures and different strain rates, Acta Mechanica Solida Sinica, 26 (**2013**) 2, 111–120, doi:10.1016/S0894-9166(13)60011-7

[23] Y. Li, C. Pan, H. Teng, J. Wang, Q. Liang, Study on middle temperature deformation behavior of solid-solution 7050 aluminum alloy based on modified J-C constitutive model, Forging & Stamping Technology, 49 (**2024**) 6, 221–226, doi:10.13330/j.issn.1000-3940.2024.06.028

[24] G. Lei, B. Wang, J. Lu, C. Wang, Y. Li, F. Luo, Effects of solid solution temperature on the microstructure and properties of 6013 aluminum alloy, Materials Chemistry and Physics, 280 (**2022**), 125829, doi:10.1016/j.matchemphys.2022.125829

[25] H. Zhao, Q. Cheng, Y. Zhao, Y. Kang, W. Zhang, L. Ye, Effect of solid solution treatment on microstructure and properties of extruded 7055 aluminum alloy, Journal of Central South University, 31 (**2024**) 1, 25–42, doi:10.1007/s11771-023-5525-z

[26] A. Rudnytskyj, P. Simon, M. Jech, C. Gachot, Constitutive modelling of the 6061 aluminium alloy under hot rolling conditions and large strain ranges, Materials & Design, 190 (**2020**), 108568, doi:10.1016/j.matdes.2020.108568

[27] J. Zhang, T. He, X. Du, Y. Huo, D. Jia, X. Chen, Effect of pre-equal channel angular pressing homogenization on microstructure and mechanical properties of as-cast 7050 Al alloy, Journal of Materials Engineering and Performance, 34 (**2025**) 12, 12174–12184, doi:10.1007/s11665-024-09950-1

[28] X. Chen, J. Wang, L. Yang, G. Zhang, Shear Specimens and Dynamic Shear Mechanical Properties of 6061-T6 Aluminum Alloy Sheets, Journal of Mechanical Engineering, 59 (**2023**) 4, 62–70, doi:10.3901/JME.2023.04.062

[29] D. Li, A. Ghosh, Tensile deformation behavior of aluminum alloys at warm forming temperatures, Materials Science and Engineering: A, 352 (**2003**) 1–2, 279–286, doi:10.1016/S0921-5093(02)00915-2

[30] W. J. Kim, J. K. Kim, T. Y. Park, S. I. Hong, D. I. Kim, Y. S. Kim, J. D. Lee, Enhancement of strength and superplasticity in a 6061 Al alloy processed by equal-channel-angular-pressing, Metallurgical and Materials Transactions A, 33 (**2002**) 10, 3155–3164, doi:10.1007/s11661-002-0301-4

[31] A. Rudnytskyj, P. Simon, M. Jech, C. Gachot, Constitutive modelling of the 6061 aluminium alloy under hot rolling conditions and large strain ranges, Materials & Design, 190 (**2020**), 108568, doi:10.1016/j.matdes.2020.108568

[32] Y. Lin, X. Chen, G. Liu, A modified Johnson-Cook model for tensile behaviors of typical high-strength alloy steel, Materials Science and Engineering: A, 527 (**2010**) 26, 6980–6986, doi:10.1016/j.msea.2010.07.061